Auger decay of the 2*p* vacancy in chlorine

M. Hrast,[1,2] A. Mihelič,[1] K. Bučar,[1] and M. Žitnik[1]
[1]*Jožef Stefan Institute, Jamova Cesta 39, 1000 Ljubljana, Slovenia*
[2]*Faculty of Mathematics and Physics, University of Ljubljana, Jadranska Ulica 19, 1000 Ljubljana, Slovenia*

(Received 2 April 2019; published 9 August 2019)

We calculate the spectra of electrons emitted upon Auger decay of the $2p$ vacancy in chlorine. The vacant atomic and ionic states are populated by a single-photon absorption from the ground state of the chlorine atom and are tested by comparing the calculated photoabsorption spectrum with the existing theoretical and experimental photoionization data. The agreement is reasonably good, although the calculated Auger decay rates and oscillator strengths of the low-lying states are overestimated due to neglect of the core polarization effects. In the absence of any published experimental result, the nonresonant L-M_{23}^2 Auger spectrum of Cl at 220 eV photon energy is compared with the Cl L-V^2 Auger spectrum of HCl, measured at 235 eV photon energy. The calculated spectator and participator resonant Auger spectra of some strongly photoexcited Cl $2p^{-1}$ states are presented for future reference.

DOI: 10.1103/PhysRevA.100.023408

I. INTRODUCTION

An accurate theoretical description of electronic states in the open-shell atoms is a challenging task. This is even more true when dealing with processes such as photoionization or Auger decay involving highly correlated states with several vacancies in the outer shells coupled to electrons residing in weakly bound orbitals. Caldwell *et al.* [1] focused on the generic problem of the chlorine $2p$ edge to study photoexcitation to atomic states with three open shells. Specifically, they studied the Cl$[2p^{-1}3p^{-1}n\ell]$ states,[1] where the weakly bound orbital $n\ell$, populated by ground-state photoexcitation, is approximately represented by a mixture of the dipole-allowed $(n \geqslant 4)s$ and $(n \geqslant 3)d$ orbitals. Although chlorine neighbors argon in the Periodic Table, its $2p$ photoabsorption spectrum is strikingly different: In contrast to a buildup of the $[2p^{-1}n(s,d)]$ Rydberg series featuring 120–140 meV linewidths while converging to the Ar $2p_{3/2,1/2}^{-1}$ thresholds [2], the chlorine photoabsorption spectrum looks rather erratic with no clear Rydberg progression and surprisingly narrow widths of the dominant low-lying $4s$ and $3d$ lines. These studies were extended by the photoelectron spectroscopy revealing positions of eight out of ten Cl$[2p^{-1}3p^{-1}]$ ionization thresholds [3]. Two theoretical papers followed soon, the first one reproducing the measured Cl$[2p^{-1}3p^{-1}]$ ionization energies within the multiconfiguration Hartree-Fock (HF) model supported by a perturbative account of the missing terms from the Breit-Pauli Hamiltonian [4]. Martins [5] launched a large-scale configuration interaction (CI) HF calculation, adding the Blume-Watson-type spin-orbit interaction term and describing the other relativistic effects by the Darwin and mass-velocity operators. The calculations reproduced the lower part of the measured spectra rather well by representing the states in the intermediate coupling scheme and describing the photoionization process within the Fano and Mies formalism, a necessary tool to account for the autoionization decay of states with the $2p_{1/2}$ vacancy whose excitation energies are above the lowest $[2p^{-1}3p^{-1}]\,^1P_1$ ionization threshold at 207.850(15) eV [3].

The most recent work in the field is the measurement by Stolte *et al.*, published in 2013 together with the relativistic Breit-Pauli R-matrix calculations of photoionization spectra close to the Cl $2p$ edge [6]. Their experiment employed an elaborate target preparation technique with the Cl_2 gas flowing through the microwave cavity to produce the atomic chlorine. Still, the contamination due to the Cl_2 background signal had to be subtracted from the measured chlorine ion yields to obtain a pure atomic signal. They also presented a theoretical photoionization spectrum, which is in a reasonable agreement with the experimental data and shows a wealth of details in each of the $Cl^+[2p^{-1}3p^{-1}]$ LSJ partial ionization cross sections.

Further implementation of the photoelectron spectroscopy would enable a direct determination of the partial cross sections, and the Auger spectroscopic studies are necessary to pin down the branching ratios of the excited states for the various decay channels. Indeed, there is no published experimental spectrum of the Auger decay of a $2p$ vacancy state in a chlorine atom and to date there is a single reference with published theoretical resonant Auger spectra of the $2p$ vacancy [5]. These calculations were pursued primarily to estimate the Cl$[2p^{-1}3p^{-1}n\ell]$ spectral widths needed to reproduce the observed photoionization spectrum, and the final states of the Auger decay were approximated by a single configuration. In this work we present theoretical resonant Auger spectra of the low-lying resonances calculated in a fully relativistic CI manner, as well as the nonresonant L-M^2 Auger spectra of different Cl^+ ionic states.

It is worth mentioning that several recent experimental studies exist of the Auger decay upon resonant photoexcitation to dissociative states in the chlorine-containing

[1]In this work we use square brackets to denote a difference with respect to the Ar closed-shell configuration $1s^2 2s^2 2p^2 3s^2 3p^6$.

molecules, involving either $1s$ or $2p$ vacancy localized on the chlorine atom [7–9]. In HCl, the dissociation can be so fast that it competes with the electronic decay of the $2p$ hole, which has a characteristic 10-fs lifetime [7]. It is likely that upon ultrafast distancing of the nuclei, an electron from the σ^* molecular orbital finds itself in an atomiclike $3p$ orbital of Cl atom before the Auger decay occurs. Consequently, the Auger spectrum of HCl looks like the L-M^2 spectrum of the argonlike chlorine Cl$[2p^{-1}]$. Its characteristic $3p^{-2}(^1S,^1D,^3P)$ multiplet structure is shifted to about 20 eV lower electron kinetic energies with respect to the Ar spectrum because of the weaker electrostatic potential of the $Z = 17$ nucleus. Replacing H with a heavier atom like C or Cl slows down the dissociation and the Cl $2p$ Auger spectrum acquires a molecular character, i.e., it involves a significant contribution from electrons ejected from a truly molecular valence orbital. For chloromethanes, Kokkonen *et al.* have shown that although in all cases the chlorine atom is bound to the carbon atom, the differences in the charge redistribution triggered by dissociation of different molecules can have a large effect on the Auger spectrum [8]. To explain these results, an elaborate theoretical treatment of the Auger decay in dissociative molecular states is required. Nevertheless, to understand the Auger data, it is useful to know the spectra in the limiting case when decay of the $2p$ vacancy primarily happens on a single Cl atom or ion. Contrary to the HCl case, one may imagine that, due to fast dissociation, an electron in the lowest unoccupied molecular orbital is pulled away from the chlorine atom so that Auger emission occurs in the $Cl^+[2p^{-1}3p^{-1}]$ ion and populates one of the Cl^{2+} final states. For most of the molecules this is an unlikely scenario as the Cl atom is more electronegative than its neighboring atom. However, it would be important to know how these Auger spectra look, to be able to detect the process in molecules where it may play a role, for example, in chlorine fluorides.

Below we present a theoretical study of the Auger decay following either Cl $2p$ photoexcitation or photoionization. The calculated photoabsorption spectrum below the $2p$ ionization threshold is compared with the results of previous experiments and calculations [3,5,6]. The calculated nonresonant L-M^2 Auger spectrum of the Cl^+ ion is compared with the observed Auger spectrum emitted by the Cl $2p$ vacancy in the HCl^+ molecular ion. The calculated resonant L-M^2 spectra are presented for some of the photoexcited atomic states with large oscillator strengths.

II. CALCULATIONS

In this work we consider all decay channels that fill the $2p$ vacancy and produce a continuum electron, both the participator and the spectator Auger processes. Figure 1 shows photoexcitation and decay pathways with channels included in the calculation.

The calculation of states and transition rates was performed by GRASP2K and RATIP-2012 codes [10,11], which are based on the relativistic multiconfigurational Dirac-Fock method. As noted before [1], the configuration interaction has a dramatic effect on the oscillator strengths for the ground-state photoexcitation of the $2p$ orbital, particularly when an electron populates the nd orbitals.

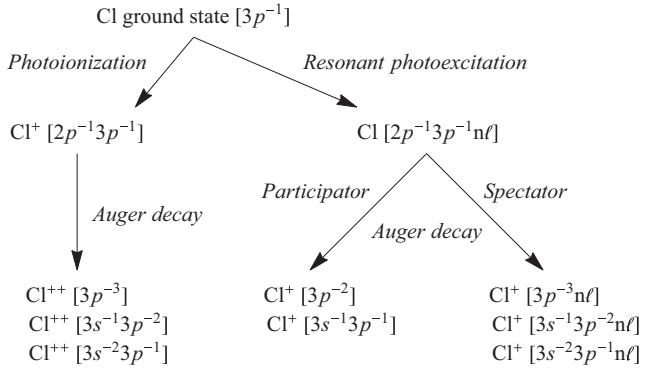

FIG. 1. Configuration states and decay channels included in the calculation.

A. State description

The state optimization was done separately for each set of configurations, marked in Fig. 1. Following Ref. [5], the $[3p^{-1}]\,^2P_{3/2}$ ground-state configuration was allowed to mix with the $[3p^{-3}3d^2]$ configuration, resulting in the 2 eV lower binding energy. This mixing was later abandoned in our calculation as there was no hope to treat the photoexcited states on the same footing due to an excessive number of required configurations. Unless stated otherwise, it is assumed that all the Cl atoms are initially in the ground state.

Ground-state photoionization populates ten $[2p^{-1}3p^{-1}]$ configuration states of the Cl^+ ion with different values of the total orbital angular momentum L, the total spin S, and the total angular momentum J. The L-M^2 Auger decay of the $2p$ vacancy in the ion populates the following states of the doubly ionized chlorine ion: five states with the $Cl^{2+}[3p^{-3}]$ configuration, ten states with the $Cl^{2+}[3s^{-1}3p^{-2}]$ configuration, and ten states with the $Cl^{2+}[3s^{-2}3p^{-1}]$ configuration. Photoionization rates were calculated for photon energy equal to 220 eV, set just above all of the $Cl^+[2p^{-1}3p^{-1}]$ thresholds. Small shifts in photon energy were found not to affect the calculated L-M^2 spectral shape significantly.

For the singly excited $Cl[2p^{-1}3p^{-1}n\ell]$ atomic states and for the $Cl^+[(3p^{-3}, 3s^{-1}3p^{-2}, 3s^{-2}3p^{-1})n\ell]$ ionic states populated by the spectator decay, configurations with $n\ell \in \{4s, 5s, 3d, 4d\}$ were mixed. This was deemed sufficient because this work is mainly concerned with the Auger decay of the lowest-lying atomic states with the $2p$ vacancy. Thus, the intermediate $Cl[2p^{-1}3p^{-1}n\ell]$ set of states consisted of 34 states with $J = 1/2$, 50 states with $J = 3/2$, and 44 states with $J = 5/2$. We found no significant mixing between the states with s symmetry, while there was considerable mixing between the states with the $2p$ electron transferred to the $3d$ or $4d$ orbital. In the spectator Auger decay of the intermediate atomic states, either the $3s$ or the $3p$ electron fills the vacancy and another $3s$ or $3p$ electron is ejected. The selected CI mixing frame leads to 272 final states of the Cl^+ ion: 96 LSJ states with the $[3p^{-3}n\ell]$ configuration, 144 states with the $[3s^{-1}3p^{-2}n\ell]$ configuration, and 32 states with the $[3s^{-2}3p^{-1}n\ell]$ configuration. The participator Auger decay populates five LSJ states with the ionic ground-state configuration $Cl^+[3p^{-2}]$ and four states with the $Cl^+[3s^{-1}3p^{-1}]$ configuration, where the $3s$ electron fills the $2p$ vacancy.

TABLE I. Assignment of peaks from Fig. 2(b). The corresponding photoexcited states of the Cl atom are denoted by $[2p_j^{-1}3p^{-1}(I)n\ell]T$, where $n\ell$ is the single-electron orbital populated by photoexcitation, I is the LS term of the $[2p_j^{-1}3p^{-1}]$ core, and T is the leading configuration term with weight w in the $L_iS_iJ_i$-coupling scheme. The calculated excitation energies E_i, spectral widths Γ_i, and total photoabsorption cross sections $\sigma_i^{\rm tot}$ are reported and compared with the observed line energies and linewidths from the experiment of Stolte *et al.* [6], tentatively assigned to the calculated transitions. The last column gives the linewidth ratio $R = \Gamma_i/\Gamma_i$ [6].

i	State	w (%)	E_i (eV)	E_i[a] (eV)	$\sigma_i^{\rm tot}$ (kb eV)	Γ_i (meV)	Γ_i[a] (meV)	R
1*a*	$2p_{3/2}\,(^1P)4s^2P_{1/2}$	72	203.3	203.9	26	81	16[b]	5.1
b	$2p_{3/2}\,(^1P)4s^2P_{3/2}$	69			60	99	16[b]	6.2
2	$2p_{3/2}\,(^3D)4s^2D_{5/2}$	61	203.7	204.2	187	27	8.5	3.2
3*a*	$2p_{3/2}\,(^3P)4s^4P_{3/2}$	46	204.0	204.8	34	400	43[b]	9.3
b	$2p_{3/2}\,(^1D)4s^2D_{3/2}$	43	204.1		29	300	43[b]	7.0
c	$2p_{3/2}\,(^1P)5s^2P_{1/2}$	51	204.2		1	574	43[b]	13.3
4*a*	$2p_{1/2}\,(^1D)4s^2D_{5/2}$	50	205.5	206.1	121	396	156[b]	2.5
b	$2p_{3/2}\,(^1P)5s^2P_{1/2}$	73			6	75	156[b]	0.48
5	$2p_{1/2}\,(^3S)4s^2S_{1/2}$	65	205.7		49	125		
6	$2p_{3/2}\,(^3D)5s^2D_{5/2}$	72	205.8	206.6	54	16	25	0.6
7	$2p_{3/2}\,(^1P)4d^2D_{5/2}$	69	206.5	206.9	35	80	28	2.8
8*a*	$2p_{3/2}\,(^3D)4d^2S_{1/2}$	43	206.9	207.4	40	26	35[b]	0.7
b	$2p_{3/2}\,(^3D)4d^2P_{3/2}$	39			45	44	35[b]	1.25
9*a*	$2p_{3/2}\,(^3D)3d^2S_{1/2}$	42	207.2	207.7	17	35	27[b]	1.3
b	$2p_{3/2}\,(^3D)3d^2D_{5/2}$	41			16	23	27[b]	0.9

[a]Reference [6].

[b]Experimental linewidths apply for the group of states.

B. Photoexcitation

For a comparison with the experimental photoionization spectrum of Stolte *et al.* [6] below the $2p$ ionization threshold, the calculated photoabsorption spectrum was broadened by a unit-area Gaussian $G(E,\Gamma_\gamma)$ with a full width at half maximum (FWHM) of $\Gamma_\gamma = 30$ meV:

$$\sigma(E) = \sum_i \sigma_i^{\rm tot} \int dE' G(E-E',\Gamma_\gamma)\mathcal{L}(E'-E_i,\Gamma_i). \quad (1)$$

In Eq. (1), $\mathcal{L}(E-E_i,\Gamma_i)$ denotes a Lorentzian with the FWHM width Γ_i, centered at the excitation energy E_i and normalized to the unit area, and E is the incident photon energy. The sum runs over all the i states accessible from the ground state by dipole interaction. The photoabsorption cross section of state i was calculated following [12],

$$\sigma_i^{\rm tot} = \frac{4\pi^2\alpha E_i S_i}{3(2J_0+1)}, \quad (2)$$

where $S_i = |\langle i||D||0\rangle|^2$ is the calculated line strength for the $0\rightarrow i$ transition [13] and J_0 is the total angular momentum of the ground state.

C. Auger decay

To present an angle-integrated Auger spectrum emitted by $Cl^+[2p^{-1}3p^{-1}]$ ionic states at photon energy $E_p = 220$ eV, a single differential cross section

$$\frac{d\sigma}{dE}(E_p) = \sum_I \sigma_I(E_p) \sum_F \frac{\Gamma_{IF}}{\Gamma_I}\mathcal{L}(E-E_{IF},\Gamma_I) \quad (3)$$

is calculated as a function of electron kinetic energy E. The sum runs over the singly charged initial (I) and doubly charged final (F) ionic states. The Auger electrons cluster at transition energies $E_{IF} = E_I - E_F$, and this is described by a sum of Lorentzians with the FWHM Γ_I, each weighted by the ratio of the partial Auger width Γ_{IF} to the total width Γ_I of the ionic state. To obtain a realistic Auger spectrum at photon energy E_p, the spectra of different ionic states are weighted by the corresponding photoabsorption cross section $\sigma_I(E_p)$. Note that the fluorescence yield of the $2p$ vacancy in Cl atom is of the order of 10^{-4}, so the fluorescence decay channel can be safely neglected [14]. Thus, for all practical purposes, the $2p$ photoionization spectrum coincides with the corresponding photoabsorption spectrum.

Finally, the resonant Auger spectrum of the ith photoexcited state is taken to be proportional to

$$A_i(\epsilon) = \sum_f \frac{\Gamma_{if}}{\Gamma_i}\mathcal{L}(\epsilon,E_{if},\Gamma_i), \quad (4)$$

where $\int A_i(\epsilon)d\epsilon = 1$, and the spectral linewidths Γ_i are reported in Table I. However, Eq. (4) gives a realistic spectral shape only for a broadband photoexcitation: Because of the resonant Raman effect, the lines can be narrower than Γ_i if the photon spectral broadening is less than the natural line broadening [15]. The use of expression (4) is also not appropriate when the lifetime interference effects are strong, i.e., when the spectral separation between two or more photoexcited states decaying to the same final state f is less than Γ_i [16]. Despite the existence of such close-lying states in the chlorine atom, the calculations lend credibility to the spectral presentation (4) by showing that they would only exceptionally decay to the same final state with comparable amplitudes.

III. RESULTS

A. Photoabsorption

The calculated photoabsorption spectrum below the lowest $Cl^+[2p^{-1}3p^{-1}]\,^1P_1$ ionization threshold is shown in Fig. 2(a)

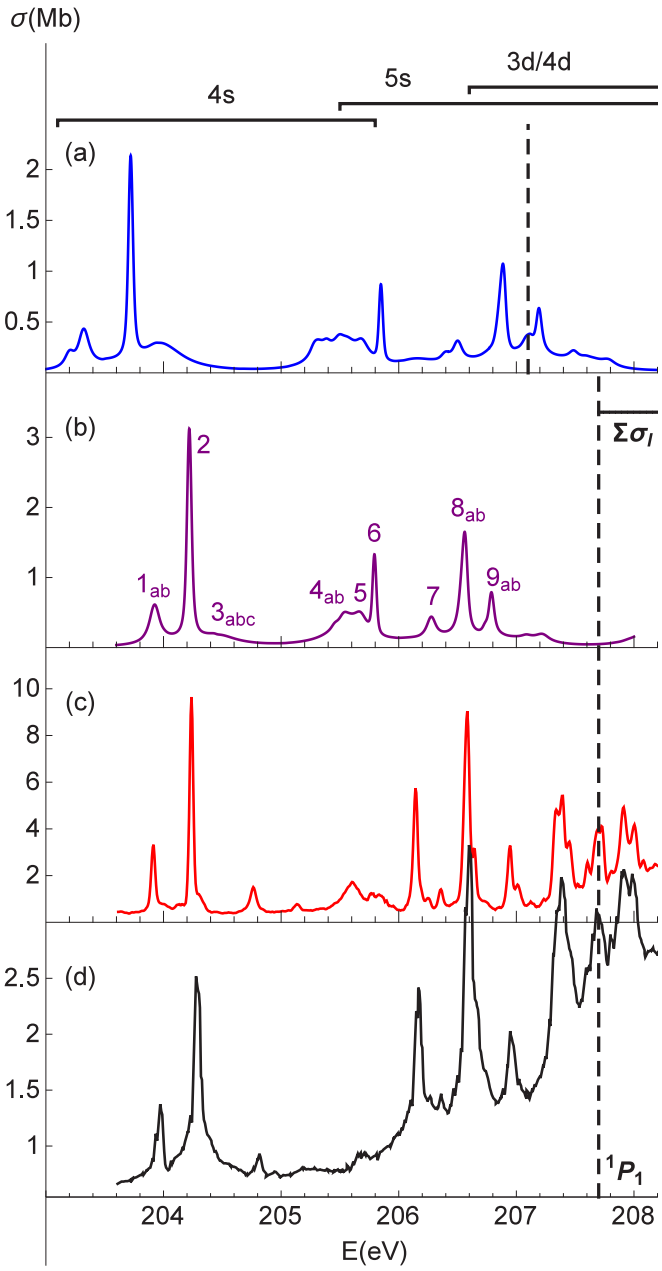

FIG. 2. (a) Calculated photoabsorption spectrum of the Cl atomic target in the statistical mixture of the ^2P ground-state doublet, (b) the shifted and scaled calculated photoabsorption spectrum where all Cl atoms are in the $^2P_{3/2}$ ground state (see the text), and experimental photoionization spectrum from (c) Stolte *et al.* [6] and (d) Caldwell *et al.* [1], put on an absolute scale by calculations in [6] and [5], respectively. The horizontal line labeled $\sum\sigma_I = 3.36$ Mb marks the calculated photoabsorption cross section at 220 eV photon energy. The vertical dashed line denotes the calculated position of the lowest $Cl^+[2p^{-1}3p^{-1}]\,^1P_1$ ionization threshold.

for atoms initially in the statistical mixture of the ground-state doublet ^2P. The most intense peaks in the spectrum are numbered in Fig. 2(b) and identified in Table I. The leading configurations of photoexcited states are also given and agree with those of Martins [5]. The states built on the $2p_{3/2}$ vacancy bear significantly more spectral intensity than those based on $2p_{1/2}$. As shown by calculations, the spin-orbit splitting amounts to 2.3, 2.0, and 1.8 eV for photoexcited states with the total angular momentum $J_i = 1/2$, $3/2$, and $5/2$, respectively.

In Fig. 2(b) the calculated spectrum is scaled linearly to align the position of peaks 1_{ab} and 8_{ab} with the position of peaks 1 and 10, respectively, measured in the experiment [6]. Effectively, this means that the spectrum in Fig. 2(a) is shifted by +0.6 eV and the values of Slater integrals determining the differences of peak positions are scaled by a factor of 0.74. A similar procedure, motivated by a comparison with the experimental data [1], was applied in the theoretical work of Martins [5] to mimic the lack of electron correlation induced by core polarization. An explicit treatment of coupling of an electron in the $n\ell$ orbital to the electrons in the $3p$ shell would require a consideration of a prohibitively large number of configurations of type $Cl[2p^{-1}3p^{-3}(n'\ell')^2n\ell]$ in the CI calculation of the photoexcited states. A single scaling factor correction is only an effective approximate solution to the core polarization problem because, as shown by Petrov *et al.*, the model short-range polarization potential results in different scaling factors for different types of Slater integrals F^k, G^k, and R^k [17].

The ratio of the calculated versus experimental Auger widths in Table I demonstrates a strong overestimation of the calculated decay rates for the lowest photoexcited states. It is known that the calculated oscillator strength depends on the form of the core polarization potential [18], and it comes with no surprise that the Auger decay rates are affected too. Interestingly, when the spectrum is plotted by combining the calculated photoabsorption cross sections with the experimentally determined linewidths, the agreement with the measured spectrum is worse compared with the case where $\sigma_i^{\rm tot}$ and Γ_i are both calculated to generate the spectrum [Fig. 2(b)]. A lower sensitivity of the peak amplitudes to the approximate treatment of core polarization may be a consequence of the fact that the peak amplitude is proportional to the area-to-width ratio $\sigma_i^{\rm tot}/\Gamma_i$, where the effect of correlations is partially canceled out. This indicates that the calculated photoexcitation cross sections of the low-lying states may be overestimated as well. However, one should also note that the convolution (due to the finite photon bandwidth) generally reduces the importance of the linewidth on the final spectral line shape and tends to generate peak amplitudes in proportion to the peak areas when the experimental broadening is significantly larger than the linewidths.

Finally, in Fig. 2(b), only the $J_0 = 3/2$ contribution is presented because our result compares better with the experimental data of Stolte *et al.* [6] when assuming that all target atoms are initially in the ground state [see Fig. 2(a)]. In fact, Caldwell *et al.*, who used microwaves to dissociate chlorine atoms in the HCl gas flow, claimed to observe no significant signal originating from the $J_0 = 1/2$ member of the ground-state doublet [1].

The two published experimental data sets are presented in Figs. 2(c) and 2(d) and generally agree with each other. They were put on an absolute scale by calculations of Stolte *et al.* [6] and Martins [5], respectively. Our calculated peak amplitudes are closer to the latter even when taking into account a minor difference in the actual experimental resolution (30 vs 40 meV). As expected, the agreement with the

TABLE II. Calculated energy positions E_I and decay widths Γ_I of ten Cl 2p ionization thresholds and the corresponding photoabsorption cross sections σ_I at 220 eV photon energy are compared with the previous results of Martins [5], Whitfield *et al.* [3], and Stolte *et al.* [6]. For each ionic state, energies E_{IF} of the strongest L-M_{23}^2 Auger transitions are reported together with the major term of the corresponding $Cl^{2+}[3p^{-3}]$ final state and the partial Auger decay width Γ_{IF}.

$Cl^+[2p^{-1}3p^{-1}]$	E_I	E_I[a]	E_I[b]		E_I[c]		σ_I	σ_I[a]	Γ_I	$Cl^{2+}[3p^{-3}]$	E_{IF}	Γ_{IF}
I	(eV)	Theor.	Theor.	Expt.	Theor.	Expt.	(Mb)	(Mb)	(meV)	F	(eV)	(meV)
$^1P_1$	207.10	208.1	207.69	207.85	207.12	207.84	0.30	0.48	13	$^2D_{5/2}, ^2P_{1/2}$	169.0	1.3
										$^2D_{3/2}$	170.1	3.2
										$^4S_{3/2}$	172.9	1.2
$^3D_3$	+0.28	+0.2	+0.23	+0.33	+0.24	+0.33	1.06	1.40	8	$^2P_{1/2}$	169.3	1.1
										$^2D_{3/2}$	170.4	2.5
$^3D_2$	+0.89	+0.9	+0.87		+0.98		0.18	0.25	85	$^2D_{5/2}, ^2P_{1/2}$	169.9	14
										$^2D_{3/2}$	171.0	24
										$^4S_{3/2}$	173.8	13
$^3S_1$	+1.28	+1.2	+1.26	+1.61	+2.04	+1.61	0.05	0.14	121	$^2D_{5/2}, ^2P_{1/2}$	170.3	21
										$^2D_{3/2}, ^2P_{3/2}$	171.4	31
										$^4S_{3/2}$	174.2	23
$^3P_2$	+1.57	+1.8	+1.95	+1.83	+2.56	+1.82	0.62	1.06	340	$^2D_{5/2}$	170.6	43
										$^2D_{3/2}, ^2P_{3/2}$	171.7	113
										$^4S_{3/2}$	174.5	56
$^3D_1$	+2.09	+1.8	+1.98		+1.41		0.01	0.22	11			
$^3P_0$	+2.21	+2.4	+2.61	+2.34	+3.27	+2.34	0.08		382	$^2P_{1/2}$	171.3	80
										$^2P_{3/2}$	172.4	88
										$^4S_{3/2}$	175.1	65
$^3P_1$	+2.73	+2.9	+3.00	+2.84	+3.48	+2.83	0.32		252	$^2D_{5/2}, ^2P_{1/2}$	171.8	43
										$^2D_{3/2}, ^2P_{3/2}$	172.9	66
										$^4S_{3/2}$	175.7	48
$^1D_2$	+3.32	+3.5	+3.71	+3.70	+4.54	+3.70	0.70		343	$^2D_{5/2}, ^2P_{1/2}$	172.4	57
										$^2D_{3/2}$	173.5	109
										$^4S_{3/2}$	176.3	6
$^1S_0$	+4.87		+5.27	+5.30	+6.53	+5.28	0.04		374	$^2D_{5/2}$	173.9	183

[a]Reference [5].
[b]Reference [3].
[c]Reference [6].

experimental data gets worse at higher photon energies due to the moderate number of configurations included in our CI calculation.

In agreement with Martins [5], we found that the $Cl^+[2p^{-1}3p^{-1}]$ ionic states are either long or short lived, depending on the LS coupling of the 2p3p vacancies. Stolte *et al.* [6] also discussed two sets of states: The first with ^1P, ^3D, or ^3S coupling leads to narrow lines exhibiting linewidths of the order of 5 meV, while the second set with ^3P, ^1D, or ^1S coupling contains broader lines with about 150 meV widths. According to Ref. [7], there are two reasons for such a behavior: (i) The broader states have an allowed monopole Auger decay route whereas the narrow states do not and (ii) the higher-lying broader states can decay to the lower-lying narrow states by exchange monopole Auger decay. The same observation applies to the photoexcited atomic states where the spectator Auger decay is by far the most probable relaxation channel. However, with the exception of the 4_{ab} peak in Table I, the broad set of lines is not prominent in the photoexcitation spectrum.

In Table II the calculated 2p photoionization thresholds, the partial photoabsorption cross sections at 220 eV photon energy, and the Auger decay rates of different Cl^+ ionic states are reported and compared with the previously published data [3,5,6]. The sum of the calculated photoabsorption cross sections for all the 2p ionization channels, $\sum_I \sigma_I(220\ \text{eV}) = 3.36$ Mb, is in good agreement with the theoretical result of 3.75 Mb at 220 eV photon energy from Ref. [6] and is close to 5.0 Mb at 212 eV, reported in Ref. [5].

B. The L-M^2 Auger spectrum

The calculated Auger decay rates of Cl^+ ionic states are expected to be more accurate than the resonant Auger decay rates because the core polarization effects are reduced in the absence of an outer-shell electron. In Fig. 3, the calculated L-M_{23}^2 Auger electron spectrum is reported at 220 eV photon energy. This is the most intense part of the Auger spectrum and is further decomposed into contributions of different ionic states, each weighted by the corresponding photoionization cross section σ_I, reported in Table II. The calculated spectrum is dominated by peaks pertaining to $^3P_2$, $^3P_1$, and $^1D_2$ ionic states with large widths, pierced by narrower lines, mostly due to the $^3D_3$ and $^1P_1$ ionic states. The assignment of the most intense peaks corresponding to transitions to the $Cl^{2+}[3p^{-3}]J$ final states is reported in Table II.

For comparison we show the measured Auger spectrum of HCl molecule at 235 eV photon energy, quite above the

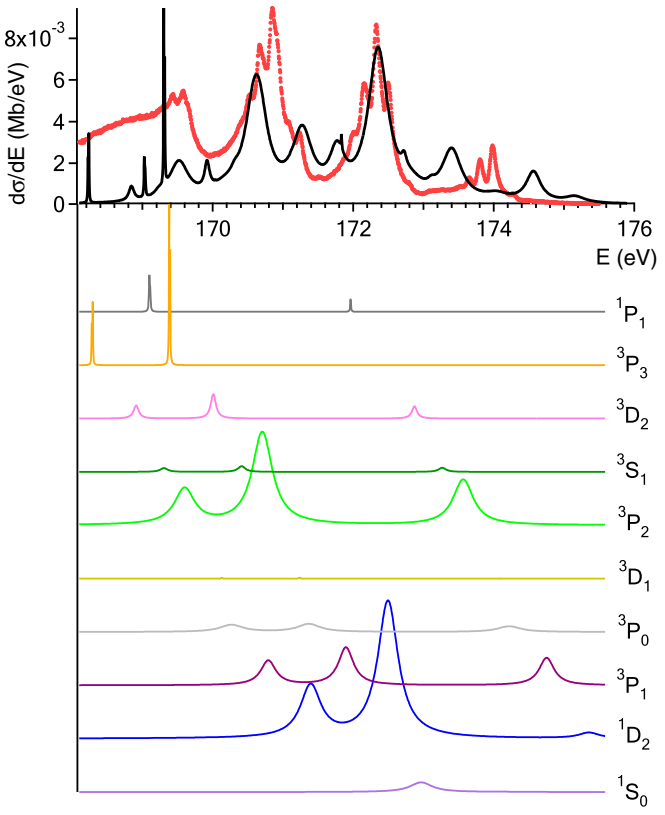

FIG. 3. Calculated L-M_{23}^2 Auger electron spectrum following photoionization of the $2p$ electron in the Cl atom (black curve) decomposed into different ionic state contributions (thin colored curves) and compared with the measured Auger spectrum of HCl at 235 eV photon energy (thick red curve) [19]. The theoretical spectra are plotted using Auger widths from Table II and then shifted by −1.1 eV to align with the experimental result.

Cl $2p$ threshold. The L-V^2 Auger spectrum was acquired with good statistics at the I411 beamline of the 1.5-GeV storage ring MAX II in Lund, Sweden, using a Scienta SES-200 hemispherical electron analyzer with 20-meV spectral resolution set to detect electrons at the magic angle [19]. The theoretical spectrum of Cl atom in Fig. 3 is shifted by −1.1 eV to tentatively align the scaled experimental spectrum. Some similarities between the two spectra are apparent, but there are also significant differences. The latter are mostly due to the vibrational structure of HCl and indicate relative stability of the final molecular states with two holes in the nonbonding $3p\pi$ valence orbitals with respect to the ultrafast dissociation triggered by photoexcitation of the σ^* state below the $2p$ ionization threshold. Another notable difference is the presence of narrow lines in the atomic spectrum.

In Fig. 4 the complete L_{23}-M^2 spectrum is shown, calculated at 220 eV photon energy. Two groups of lines at lower energies appear due to participation of the chlorine $3s$ electrons in the Auger decay. The lines in the 148–165 eV energy range almost double the total Auger yield and signal the population of the $Cl^{2+}[3s^{-1}3p^{-2}]$ final states, while close to 140 eV, there is a weak contribution of the $Cl^{2+}[3s^{-2}3p^{-1}]$ final states.

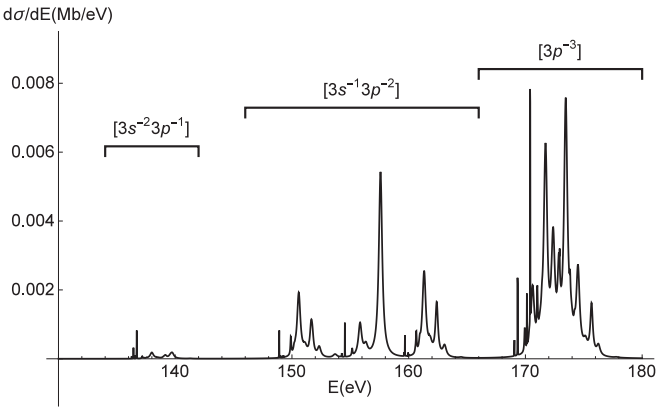

FIG. 4. Calculated L-M^2 Auger spectrum of the Cl $2p$ vacancy at 220 eV photon energy.

C. Resonant L-M^2 Auger spectra

In Fig. 5 we present the calculated resonant Auger spectra for some of the atomic states with the $2p$ vacancy that are gathered in Table I. According to Eq. (4), each spectrum is normalized to 1, although the actual electron yield also

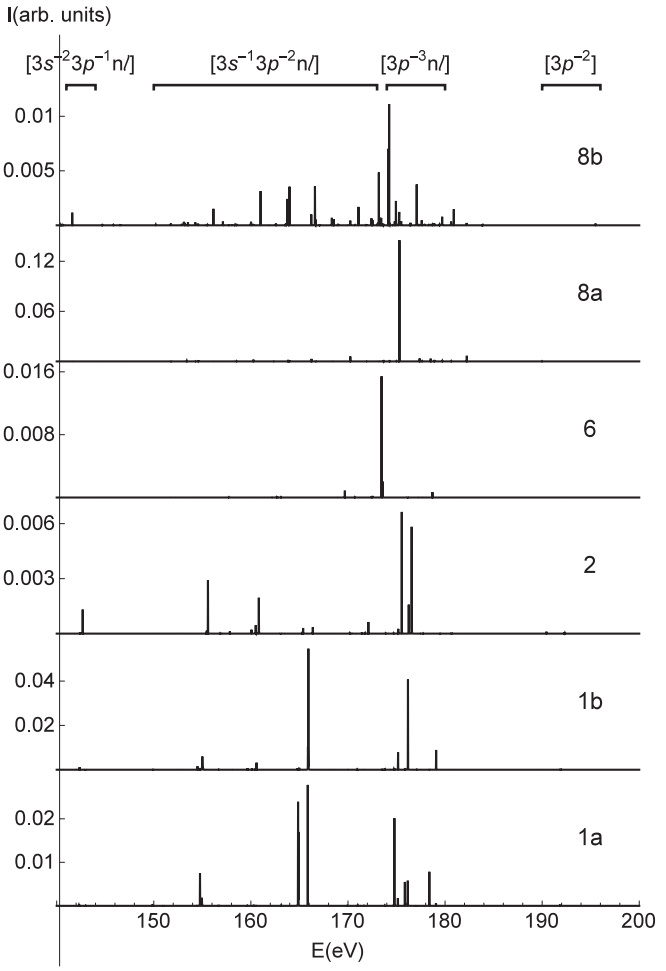

FIG. 5. Calculated resonant Auger spectra of the Cl atom, emitted by some strongly photoexcited states with a $2p$ vacancy, marked in Fig. 2(b) and described in Table I.

depends on the photoabsorption cross section of the selected atomic state. In all the resonant Auger spectra the lines are grouped in four distinct spectral intervals, marked at the top of Fig. 5. The participator Auger decay leads to the $Cl^+[3p^{-2}]$ final states and generates lines close to 192 eV. As expected, the spectator lines are shifted upward with respect to the nonresonant Auger decay: The 173–180 eV energy range covers the $Cl^+[3p^{-3}n\ell]$ final states, in the 150–173 eV range the $Cl^+[3s^{-1}3p^{-2}n\ell]$ final states are populated, and the lowest lines close to 142 eV are signaling transitions to the $Cl^+[3s^{-2}3p^{-1}n\ell]$ final states. Consistent with the results in Ref. [5], only about 1% of the excited atomic state population is found to decay by the participator Auger transition. As evident from Fig. 5, the resonant Auger spectra strongly depend on the excited state. Since there are significant differences also between the theoretical spectra for physically the same excited state [e.g., compare Fig. 4(a) in [5] with our result for peak 2 in Fig. 5], this calls for an experimental verification to provide a solid ground for the proper line assignments.

IV. CONCLUSION

We presented a theoretical study of the Auger decay of the $2p$ vacancy in the chlorine atom. To test the quality of the initial states, the calculated photoabsorption spectrum below the lowest $2p$ threshold was compared with the previous theoretical and experimental data. After application of a small energy shift and after quite significant scaling of the calculated peak positions, reasonable agreement was obtained for the resonant part of the spectrum. A clear overestimation of the calculated Auger widths for the low-lying states is attributed to the lack of treatment of core polarization. As the missing correlations in our model may have caused an overestimation of oscillator strengths for transitions from the ground state too, the calculated spectral shape still agrees quite well with the experimental data. Above the $2p$ ionization thresholds at 220 eV photon energy, the polarization effect is diminished and the calculated photoionization cross section agrees well with the previously determined theoretical values. Similar to photoabsorption, the calculated nonresonant L-M^2 Auger spectrum of Cl shows two types of lines, depending on the $2p$-$3p$ vacancy coupling in the initial state. The first group with the linewidths in the 100-meV range dominates the L-M^2 spectrum and there is the second group of narrow lines present with an order of magnitude smaller widths.

In the absence of the corresponding experimental data, the calculated L_{23}-M_{23}^2 atomic spectrum was compared with the measured L-V^2 spectrum of HCl. Although there is a match between the two regarding the gross spectral features, the molecular spectrum clearly exhibits vibrational line progressions triggered by a considerable change of the molecular potential caused by an Auger transition. On the other hand, the chlorine spectrum is pierced by the narrow atomic lines, completely absent from the HCl spectrum. Such a spectrum might be observed for Cl-X molecule by looking at the Cl^{2+}-Auger electron coincidences if the potential dissociation would result in ultrafast distancing of the $2p^{-1}$ Cl^+ ion from the X^- ion. To motivate further experimental work with chlorine atoms, the calculated resonant L-M^2 Auger spectra were presented for some strong $2p$-photoexcited atomic lines.

ACKNOWLEDGMENT

This work was supported by Program No. P1-0112 of the Slovenian Research Agency.

[1] C. D. Caldwell, M. O. Krause, R. D. Cowan, A. Menzel, S. B. Whitfield, S. Hallman, S. P. Frigo, and M. C. Severson, Phys. Rev. A **59**, R926 (1999).
[2] G. C. King, M. Tronc, F. H. Read, and R. C. Bradford, J. Phys. B **10**, 2479 (1977).
[3] S. B. Whitfield, S. Hallman, M. O. Krause, C. D. Caldwell, and R. D. Cowan, Phys. Rev. A **60**, R1747 (1999).
[4] N. J. Wilson, K. L. Bell, and A. Hibbert, J. Phys. B **33**, L341 (2000).
[5] M. Martins, J. Phys. B **34**, 1321 (2001).
[6] W. C. Stolte, Z. Felfli, R. Guillemin, G. Öhrwall, S.-W. Yu, J. A. Young, D. W. Lindle, T. W. Gorczyca, N. C. Deb, S. T. Manson, A. Hibbert, and A. Z. Msezane, Phys. Rev. A **88**, 053425 (2013).
[7] O. Travnikova *et al.*, Phys. Rev. Lett. **116**, 213001 (2016).
[8] E. Kokkonen, K. Jänkälä, M. Patanen, W. Cao, M. Hrast, K. Bučar, M. Žitnik, and M. Huttula, J. Chem. Phys. **148**, 174301 (2018).
[9] K. F. Alcantara, A. B. Rocha, A. H. A. Gomes, W. Wolff, L. Sigaud, and A. C. F. Santos, J. Phys. Chem. A **120**, 6728 (2016).
[10] P. Jönsson, X. He, C. F. Fischer, and I. P. Grant, Comput. Phys. Commun. **177**, 597 (2007).
[11] S. Fritzsche, Comput. Phys. Commun. **183**, 1525 (2012).
[12] M. Aymar, C. H. Greene, and E. Luc-Koenig, Rev. Mod. Phys. **68**, 1015 (1996).
[13] C. Froese-Fischer, T. Bragge, and P. Jönsson, *Computational Atomic Structure—An MCHF Approach* (Institute of Physics, Bristol, 1997).
[14] M. O. Krause, J. Phys. Chem. Ref. Data **8**, 307 (1979).
[15] A. Kivimäki, A. Naves de Brito, S. Aksela, H. Aksela, O.-P. Sairanen, A. Ausmees, S. J. Osborne, L. B. Dantas, and S. Svensson, Phys. Rev. Lett. **71**, 4307 (1993).
[16] M. Žitnik, M. Kavčič, K. Bučar, A. Mihelič, and R. Bohinc, J. Phys.: Conf. Ser. **488**, 012014 (2014).
[17] I. Petrov, V. Sukhorukov, M. Ruf, D. Klar, and H. Hotop, Eur. Phys. J. D **62**, 347 (2011).
[18] T. Brage and C. Froese Fischer, Phys. Scr. **45**, 43 (1992).
[19] R. Püttner, V. Pennanen, T. Matila, A. Kivimäki, M. Jurvansuu, H. Aksela, and S. Aksela, Phys. Rev. A **65**, 042505 (2002).